



OPEN

SUBJECT AREAS:

APPLIED PHYSICS

SENSORS

SEMICONDUCTORS

PHOTONIC DEVICES

Solution-Processed Nanoparticle Super-Float-Gated Organic Field-Effect Transistor as Un-cooled Ultraviolet and Infrared Photon Counter

Yongbo Yuan¹, Qingfeng Dong¹, Bin Yang¹, Fawen Guo¹, Qi Zhang², Ming Han² & Jinsong Huang¹Received
21 June 2013Accepted
27 August 2013Published
19 September 2013Correspondence and
requests for materials
should be addressed to
J.H. (jhuang2@unl.
edu)¹Department of Mechanical and Materials Engineering and Nebraska Center for Materials and Nanoscience, University of Nebraska-Lincoln, Lincoln, Nebraska 68588-0656, USA, ²Department of Electrical Engineering, University of Nebraska-Lincoln, Lincoln, Nebraska 68588-0656, USA.

High sensitivity photodetectors in ultraviolet (UV) and infrared (IR) range have broad civilian and military applications. Here we report on an un-cooled solution-processed UV-IR photon counter based on modified organic field-effect transistors. This type of UV detectors have light absorbing zinc oxide nanoparticles (NPs) sandwiched between two gate dielectric layers as a floating gate. The photon-generated charges on the floating gate cause high resistance regions in the transistor channel and tune the source-drain output current. This “super-float-gating” mechanism enables very high sensitivity photodetectors with a minimum detectable ultraviolet light intensity of 2.6 photons/ $\mu\text{m}^2\text{s}$ at room temperature as well as photon counting capability. Based on same mechanism, infrared photodetectors with lead sulfide NPs as light absorbing materials have also been demonstrated.

High sensitivity photodetectors and photon counters with a resolution at the photon level are critical in many civilian and military applications, including quantum cryptography^{1,2}, imaging at extremely low levels of ambient illumination, Light Detection and Ranging (LIDAR)³⁻⁵, space exploration^{6,7}, and medical imaging^{8,9}. The highly sensitive photodetectors in use today, such as photomultiplier tubes (PMTs) or avalanche photodiodes (APDs), combined with discriminators and associated electronics, have shown single-photon counting capability. Despite their high detectivity, the application of PMTs in many fields, such as laser radar imaging¹⁰ and medical imaging, is limited. This is due to their large, fragile vacuum tube structure, susceptibility to a magnetic field, and demand for a high driving voltage of above 1,000 volts. The quantum efficiency of a PMT is usually less than 20% in UV/blue and less than 5% in the red wavelength regime¹¹. APDs operating in the Geiger mode^{12,13} have shown much higher quantum efficiency than PMTs in the visible range, with a spatial resolution as small as 100 micrometers and a lower bias of several hundred volts^{12,14,15}. However, the Geiger mode APD suffers from high multiplication noise and after-pulse dead time problems¹⁶⁻¹⁸. New versatile applications have been pushing the development of a new generation of photodetectors with higher detectivity, un-cooled, higher resolution, better flexibility, and integration to silicon technology, all of which will be accomplished with better yield and lower manufacturing/operating costs.

Recent advancements in light detection technologies have been shown to absorb the nanomaterial revolutions of the last decade, e.g., a quantum dot single-photon detector (QDSPD) has been developed by Shields, Yablonoitch, and Mirin for single photon detection¹⁹⁻²². These QDSPDs used a layer of indium arsenide QDs embedded in a thick gallium arsenide layer between the gate dielectric layer and the channel of a field effect transistor (FET) to trap the photo-generated holes in the GaAs layer¹⁹⁻²². The trapped holes in the QDs screen the gate voltage and thus act as an optical addressable floating gate, resulting in a persistent change in the channel current. However, these QDSPDs require expensive and slow epitaxial growth in ultrahigh vacuum¹⁹⁻²¹, and the QDSPDs only work at an extremely low temperature of ~ 4 K in order to confine charges in QDs. It is unlikely these QDSPDs can be widely employed for low-cost applications. On the other hand, solution-processed devices made of organic semiconductor materials, inorganic nanoparticles (NPs), or nanocomposite materials have provided a critical step for low-cost, high performance photodetectors²³⁻²⁸. So far, nanomaterials, such as lead sulfide colloidal QDs, cadmium selenide colloidal NPs, and zinc oxide (ZnO) NPs and nanowires, have been



widely used in the photodetectors. However, most of the reported solution-processed photodetectors, based on a photoconductor or photodiode mechanism, only show minimum detectable light intensities of around $10^{-8} \sim 10^{-5} \text{ W/cm}^2$ ^{27,29–32}. In this manuscript, we report a new type of solution-processed organic field-effect transistor (OFET) as a highly sensitive un-cooled photodetector. The OFET integrates ZnO NPs sandwiched between two dielectric layers under the channel layer, and uses the photo-generated, confined electrons to tune the channel current. A huge photoconductive gain, as well as photon number memorizing and counting capability, was enabled by a novel super-float-gating mechanism. The minimum detectable ultraviolet light intensity of 2.6 photons/ $\mu\text{m}^2\text{s}$ ($1.5 \times 10^{-10} \text{ W/cm}^2$) was demonstrated.

Results

Device working principle and device performance. The nanoparticle super-gated organic field-effect transistor (NPSGOFET) photon counter is a bottom-gate, top-contact type OFET comprised of a photoactive ZnO NPs layer sandwiched between two dielectric layers, as shown in Figure 1a. A highly doped silicon (Si) wafer was used as both substrate and gate. The bottom dielectric layer was a thermal growth silicon oxide (SiO_2) layer with a thickness of 200 nm, and the top dielectric layer was a very thin layer of polystyrene (PS), on which was an organic semiconductor layer made of either trimethyl-[2,]quarter-thiophen-5-yl-silane (4T-TMS) or pentacene.

The very thin embedded PS dielectric layer was formed by the vertical phase separation of a 4T-TMS:PS blend after drop coating (See the details in the Experiment section). The corresponding scanning electron microscope (SEM) cross-section image of the device is shown in Figure 1b, where the ZnO NPs layer, PS layer, and 4T-TMS layer can be clearly identified. The optical response spectrum is determined by the ZnO NPs layer. Figure 1c shows the absorption spectrum of the ZnO NPs layer of 60 nm thick, where an optical band gap of 3.4 eV for the ZnO NPs can be identified. The thickness of this PS layer was controlled to be around 10 nm, which was adjusted by changing the ratio of the 4T-TMS:PS blend.

The working process of the NPSGOFET photon counter is schematically shown in Figure 1d. The photon counter works naturally at the ON-state. In the dark, the ZnO NPs layer, as well as the PS layer, acts as insulating dielectric layer. The holes injected from the source electrode are built up at the 4T-TMS/PS interface because of the insulating property of PS and the large energy difference between the highest occupied molecular orbital (HOMO) of 4T-TMS (-5.3 eV) and the valence band of ZnO (-7.6 eV). Driven by the source-drain voltage, the carriers transport laterally to the drain electrode. The absorption of UV photons by 4T-TMS and PS is small due to their large bandgap and small thickness. Incident UV photons excite electron-hole pairs in the ZnO NPs layer. Under the applied negative gate bias, the electrons sweep crossing the ZnO NPs layer and are confined at the ZnO/PS interface. The confined electrons at the ZnO/PS interface impose a trapping effect to the transporting

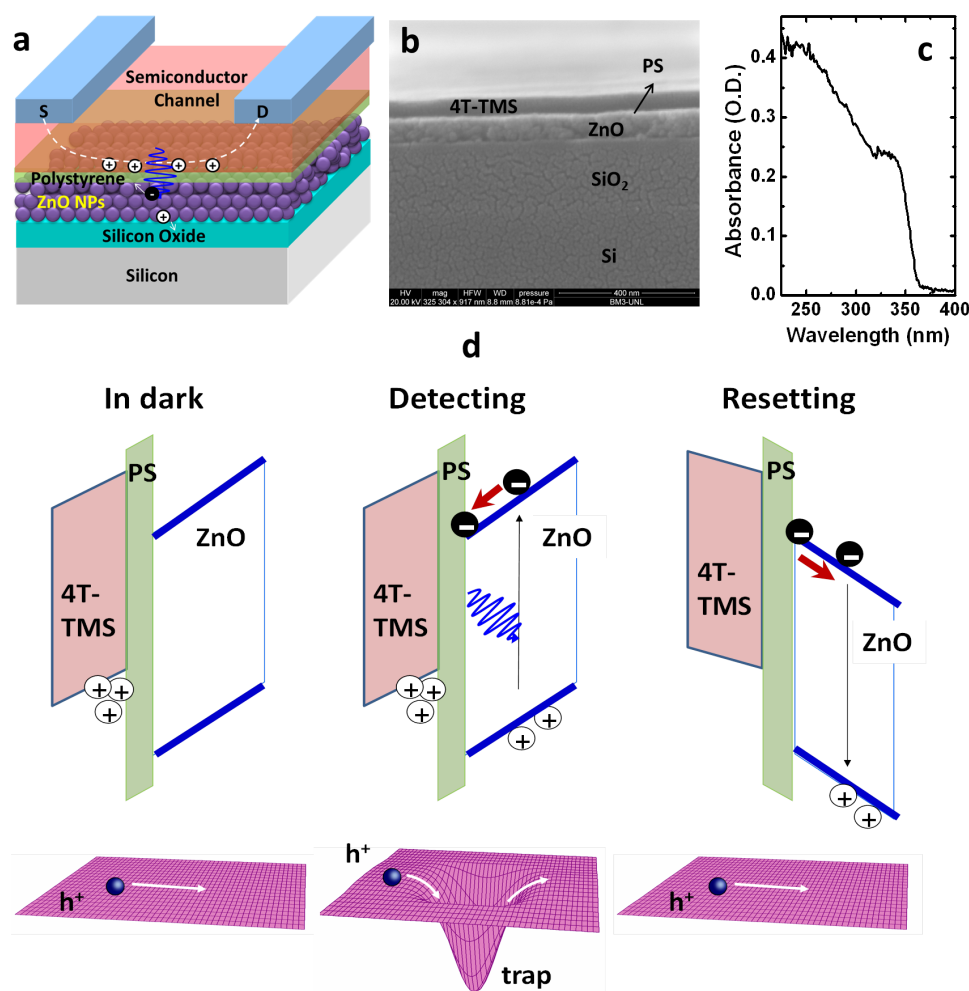


Figure 1 | (a) Device structure of NPSGOFET photodetector; (b) SEM cross-section image of the NPSGOFET photodetector; (c) absorption spectrum of the ZnO NPs photo-active layer; (d) schematic illustration of the detecting process and resetting process of the NPSGOFET photodetector.



hole carriers in the nearby semiconductor channel by columbic attraction, and thus result in a reduced source-drain output current (ΔI_{SD}) in the OFETs. The ΔI_{SD} is correlated to the density of photo-generated confined electrons at the ZnO/PS interface, and thus that of incident light intensity. The confined electrons at the ZnO/PS interface can be held for a very long time by the applied gate electric field without recombination. Hence the ΔI_{SD} persists even after the incident light is turned off. This is a major difference between our NPSGOFET photon counter and conventional photoconductor or diodes in which the current signal decays quickly once the light is off^{19–22}. In the NPSGOFET, the ΔI_{SD} is determined by the amount of absorbed photons rather than the intensity of the light, so that the device works in a photon-counting mode. This photon counter can count incident photons continuously and can be reset by a reserved gate bias pulse. Under a reserved gate bias, the electrons at the ZnO/

PS interface move toward the holes in the ZnO NPs layer and recombine with them. As a result, the photon-induced traps disappear and the channel current resumes its initial value.

Figure 2a show the typical transfer curve of the NPSGOFET device in the dark and under UV illumination. The covering of ZnO NPs with a thin layer of PS is critical for the NPSGOFET photon counter. One of its functions is to flatten and encapsulate the surface of the ZnO NPs layer so that the hole carriers are not trapped by the surface defects on the ZnO NPs and the NPSGOFET can work as a normal transistor device in the dark. The calculated hole mobility of the 4T-TMS-based transistor in the dark is around $0.065 \text{ cm}^2/\text{Vs}$, which is comparable to the reported data^{33,34}. When the device was illuminated by UV light, the channel current dropped immediately. No channel current change was observed when the channel region was illuminated by visible light (400 ~ 700 nm), which confirms that the

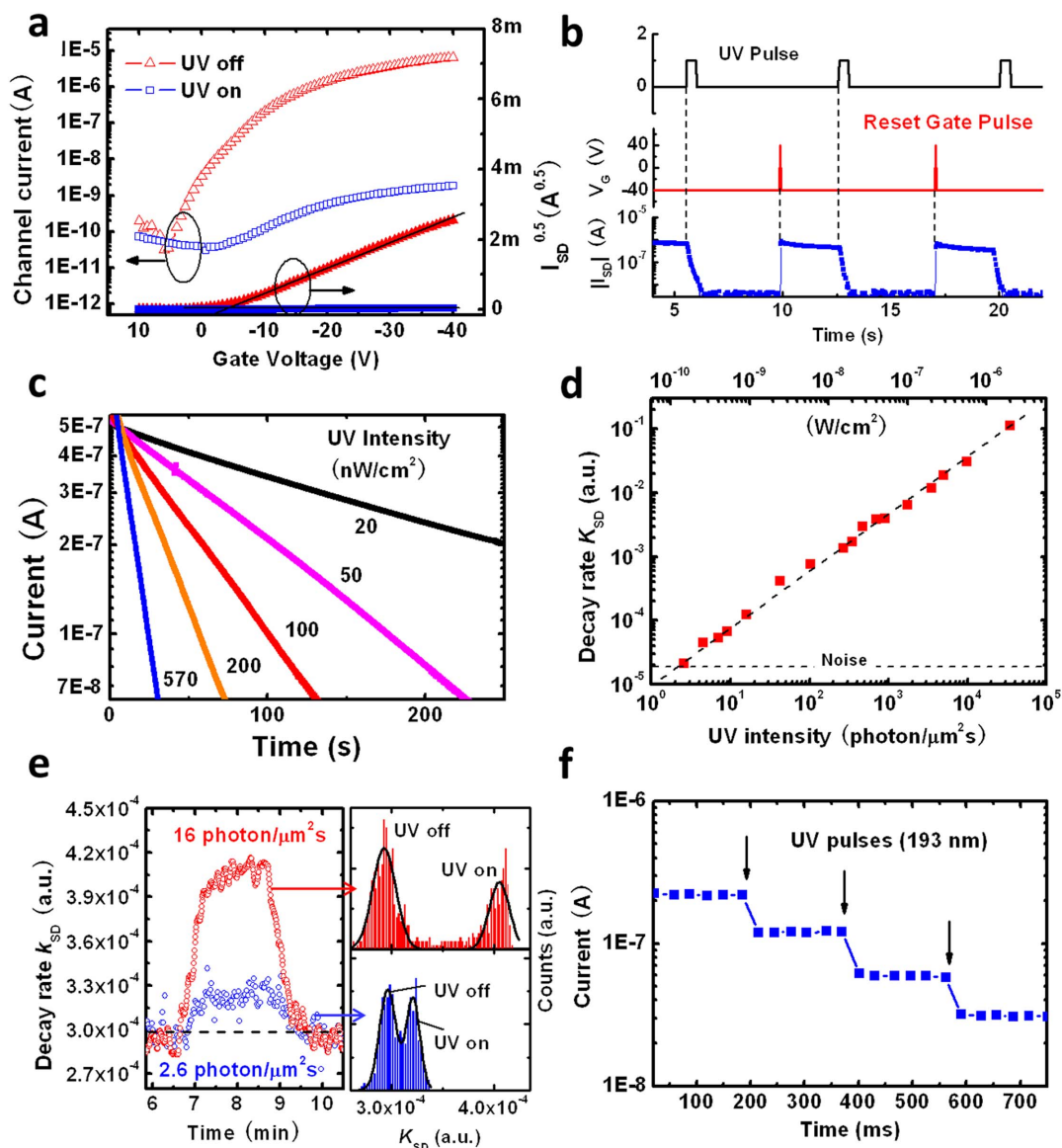


Figure 2 | (a) The transfer characteristics of the NPSGOFET photodetector in the dark (red) and under UV illumination (blue); (b) detecting and resetting of the NPSGOFET detectors under UV pulses and positive gate voltage pulses, respectively; (c) exponential channel current decay of the NPSGOFET devices under different UV light intensities; (d) the channel current decay rate as a function of the incident light intensity ranging from 2.6 photons/ $\mu\text{m}^2\text{s}$ to 3.5×10^4 photons/ $\mu\text{m}^2\text{s}$; (e) decay rate of the NPSGOFET photodetector at a weak UV power intensity of 2.6 photons/ $\mu\text{m}^2\text{s}$ and 16 photons/ $\mu\text{m}^2\text{s}$, respectively; the histograms of the current decay rate at the corresponding UV light intensities are also shown; (f) continuous photon counting of the NPSGOFET photodetector under UV (193 nm) pulses with a pulse width of 12 nanosecond and interval of 200 ms. The response speed was limited by the current measurement setup.



current variation of the OFET was caused by the absorption of UV light by the large bandgap ZnO NPs. The photon detecting and resetting of the NPSGOFET was demonstrated by recording the ΔI_{SD} under the illumination of a train of UV light pulses which was followed by a reversed gate bias pulse after each light pulse. As shown in Figure 2b, a UV light pulse with a duration of 0.5 seconds caused a ΔI_{SD} from 700 nA to 5 nA; and a ~ 40 ms reverse bias pulse can recover the I_{SD} to its initial value so that the NPSGOFET device has a standard “optical write/electrical reset” working process. Actually, the NPSGOFET device can also be partially reset by just turning off the gate voltage, because turning off the gate bias releases the confined electrons to the ZnO layer. An additional positive gate voltage leads to a fast and complete resetting. The detector show increased resistance (decreased current) by illumination, which requires unique read-out circuits with a) mirror circuit scheme for the current cancellation; or b) converting the device resistance change into voltage output change^{35–37}. Such read-out schemes are also used in other ultra-sensitive photodetectors such as superconducting single-photon detectors which have a similar response to light.

To evaluate the sensitivity and linear dynamic range of this type of photodetector, the variations of I_{SD} under different UV light intensity was studied, where the different UV light intensities were generated by a gallium nitride (GaN) light emitting diode (LED) (emission peak at 345 nm) and attenuated with a set of neutral density filters (Figure 2c). Under a constant UV light intensity, it was found that the I_{SD} decreased exponentially with time, because the photodetector kept absorbing and counting photons. A stronger UV intensity results in a faster decay rate (decay rate is defined as $k_{SD} = -d\log(I_{SD})/dt$). There is a background I_{SD} decay of the device in the dark, whose fluctuation determines the lowest light intensity that can be measured (or noise equivalent power, (NEP)). For a better understanding of the relationship between the current decay rates and the UV light intensity, we plotted the k_{SD} obtained as a function of the UV intensity in Figure 2d. The k_{SD} linearly increases with the incident UV light intensity in over four orders of magnitude from 2.6 photons/ $\mu\text{m}^2\text{s}$ to 3.5×10^4 photons/ $\mu\text{m}^2\text{s}$.

The Figure 2e show the k_{SD} of the NPSGOFET under a rectangular UV light pulse with a light intensity of 2.6 photons/ $\mu\text{m}^2\text{s}$ and 16 photons/ $\mu\text{m}^2\text{s}$, respectively, demonstrating its capability in weak light detecting. The distribution of the current decay rate in the dark or under weak UV light (2.6 photons/ $\mu\text{m}^2\text{s}$ and 16 photons/ $\mu\text{m}^2\text{s}$, respectively) is shown in Figure 2d. The device have not approach single photon counting yet because at its minimum detectable power intensity level (2.6 photons/ $\mu\text{m}^2\text{s}$, i.e. 0.15 nW/ cm^2) it requires an integration of tens of second to distinguish the signal from noise (corresponding to ~ 100 photons/ μm^2). This low level light intensity is among the lowest detectable light intensity by any un-cooled solid state UV photodetectors^{23,24,38}. It should be noted that the minimum detectable light intensity is much smaller than that of the UV photodetector with a nanostructured ZnO photoconductor^{27,29,39}, due to the high gain from the super-float-gating mechanism inherent to the NPSGOFET photon counter. The high sensitivity of these photodetector originates from the large photoconductive gain because a sufficient supply of charge is provided by the source electrode and the current change is due to the photo-induced conductivity change. The long recombination lifetime of the confined electrons theoretically can induce a very large gain to the NPSGOFET.

To demonstrate the light-pulse-counting capability of this type of photodetector, the ΔI_{SD} under a train of nano-second UV pulses was recorded and is shown in Figure 2f. The UV light pulse train, with a pulse width of 12 ns and an interval of 200 ms, was generated by an excimer UV laser (BraggStar Industrial LN 1000). Since no recovery period is required after each photon event, the NPSGOFET can count photons continuously without dead time²². The I_{SD} decreases step by step upon each incident light pulse, and the I_{SD} keeps

constant between each light pulse. This unique device behavior enables the counting of light pulses with a single device without sophisticated electronics which may find potential application in optical communication. The device response time is shorter than 30 ms, which is limited by our current measurement system. On the other hand, the unique “memory” function of such photodetectors enables the separation of light detection and signal readout so that the electronics do not need to have a quick read out speed, which can be important in applications where the total incident photon numbers are concerned, such as radiation detection²².

Super-gating mechanism. Similar to the QDSPD, the large photoconductive gain in the NPSGOFET gives the large signal output (ΔI_{SD}) per incident photon and enables the weak light detection close to the single-photon level. According to a previous analysis of QDSPD, a linear variation of transistor output current with the incident photons is expected if the charged ZnO NPs only work as a floating gate to tune the apparent gate bias to the semiconductor layer:

$$\Delta I_{SD} = g_m \frac{qD}{\epsilon} N_{ph} \quad (1)$$

where g_m is the transconductance of the transistor at a fixed gate bias, q is the element charge, D is the distance between the gate and the QD layer, ϵ is the electric permittivity of the space materials, and N_{ph} is number of absorbed photons. But the NPSGOFET have an exponential dependence of ΔI_{SD} with the amount of absorbed photons: $\Delta I_{SD} \propto \exp(-N_{ph})$. It is then expected that the charged ZnO NPs close to the 4T-TMS/PS interface play additional roles in addition to their function as a floating gate to change the effective gate bias. To better understand the unprecedented high sensitivity of the NPSGOFET photon counter at room temperature, a device model was proposed to explain the exponential decrease of the current under constant illumination.

The exponential I_{SD} decays can be explained by the trap-induced carrier mobility loss in the organic semiconductor channel of the OFET. The I_{SD} through the OFET in the saturation regime can be described by

$$I_{SD} = \frac{\mu C_i W}{2L} (V_g - V_t)^2 \quad (2)$$

where μ , C_i , W , L , V_g and V_t are the hole mobility, specific dielectric capacitance, channel width, channel length, gate bias, and threshold voltage, respectively⁴⁰. The mobility of the carriers (holes in 4T-TMS) is very sensitive to the traps with an exponential dependence^{41,42},

$$\mu \propto \exp(-\Delta E_{tr}/kT) \quad (3)$$

where ΔE_{tr} is the average energy trap depth caused by the columbic interaction between the confined electrons at the PS/ZnO interface and the transportin holes in the channel layer, which is schematically illustrated in Figure 3a. It should be noted that the extremely sensitive response of the carrier mobility of organic semiconductors to energy traps was also applied for other types of detectors, such as chemical sensors^{43–45}. Such columbic interaction of the channel carriers and confined charges was not considered in QDSPDs previously because of the large separation between them in those devices (e.g. 100 nm)¹⁹. However, it becomes important in changing the current in the channel of NPSGOFETs because of: 1) the very thin separation layer between them, which is the thickness of PS layer on the order of 5 \sim 20 nm and 2) the low dielectric constant of PS ($\epsilon_r = 2.6$).

Each confined electron at the PS/ZnO interface imposes a potential well for the transporting hole carriers in the organic semiconducting channel due to the columbic force between them. The average trap depth by all of the generated traps is expected to be proportional to incident photons, or generated traps density ($n_{tr}(t)$) at the ZnO/PS interface, as well as the trap depth of each individual trap (ΔE_{max} , Figure 3a)

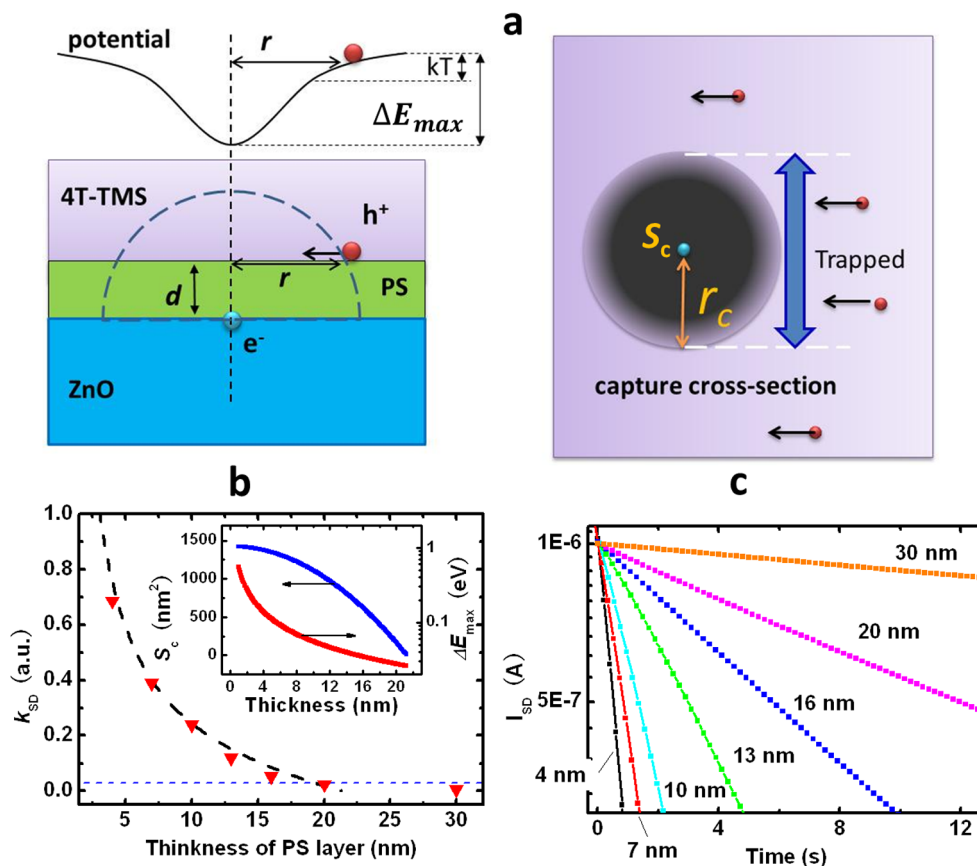


Figure 3 | (a) Schematic illustration of the depth and cross-section of the potential well caused by photo-induced confined electrons; (b) calculated channel current decay rate from the super-float-gating mechanism (dash line), the measured decay rate of the NPSGOFET device as a function of the PS layer thickness was also shown (triangle). The inset shows the cross-section and trap depth of the potential well as a function of the PS layer thickness. (c) variation of I_{SD} of the NPSGOFET photodetector with different PS layer thickness.

$$\Delta E_{tr}(t) = c\Delta E_{max}S_c n_{tr}(t) \quad (4)$$

where $n_{tr}(t) = aPt$, which was determined by UV light intensity (P , in a unit of photons/ $\mu\text{m}^2\text{s}$), the illuminating time (t), and the quantum efficiency (a) of the trap formation by the incident photons; S_c is the cross-section of each trap defined in Figure 3a, and c is a constant describing how each individual trap contributes to the average trap depth. Therefore, one can derive

$$I_{SD}(t) = I_0 \exp\left(-\frac{ac\Delta E_{max}S_c}{kT}Pt\right) \quad (5)$$

where I_0 is the initial channel current. From Equation (5), we can immediately determine the reason for the exponential decrease of the channel current under constant UV illumination and that the decay rate k_{SD} is proportional to the UV light intensity ($k_{SD} = (ac\Delta E_{max}S_c/kT)P$). It is consistent with the experimental result (Figure 2b–e).

Based on the super-float-gating mechanism, the thickness of the PS layer plays an important role in determining the sensitivity of the NPSGOFET device. At a given trap density, a decreased PS thickness gives an increased hole capture cross-section area and an increased average trap depth, as illustrated in Figure 3a, both increasing k_{SD} . The S_c , ΔE_{max} , and k_{SD} of the devices with varied PS thickness, from 30 nm to 5 nm, were calculated (see the method) and are shown in Figure 3b. As can be seen from this figure, the current decay rate of the NPSGOFET device (i.e., sensitivity of such photodetectors) increased dramatically when the PS thickness was less than 20 nm.

To verify this simulation, a series of devices with varied PS thickness were fabricated. For a better control of the PS thickness, the PS layer was spin coated from a pure PS solution. Then the semiconducting

layers (pentacene) were thermally deposited on the PS surface. The current decay of the devices with different PS thicknesses under a UV light of $3 \mu\text{W}/\text{cm}^2$ is shown in Fig. 3c, and the device output current decay rate is also plotted in Figure 3b. The results clearly show that the device performance is very sensitive to the thickness of the PS layer. The experimental results agree with the predicted k_{SD} very well with a single fitting parameter c of 0.013.

The NPSGOFET device still shows a weak response under UV light when the PS layer exceeds 30 nm, probably because other mechanisms also contribute to the detection, such as a regular floating-gate mechanism. The current changes due to the floating-gate mechanism, estimated from Eq. (1), are also shown in Figure 3c, which is ten times lower than the super-float-gating mechanisms when the PS is thinner than 10 nm. This analysis clearly shows how the thickness of the PS layer determines the device's sensitivity. It should be noted that the transistor channel current is determined by the channel width to length ratio (W/L) rather than channel area, and the output current decay rate k_{SD} is independent of the device area. It means that different from photodiodes or photoconductors, the signal (ΔI_{SD}) of NPSGOFET devices does not scale with device area. It is very attractive for the application of photodetector arrays in which a high resolution can be achieved by scaling down the device size without compromising sensitivity.

Effect of trapped electrons and infrared photodetector demonstration. In order to further confirm the super-gating mechanism and the universal application of such a device structure, an UV and infrared (UV-IR) photodetector based on same mechanism has been fabricated. Lead sulfide (PbS) NPs were synthesized with a tunable



size from 2 to 6 nm which extended the absorption of the active layer from UV to near infrared region⁴⁶. PbS NPs with size of 3–4 nm, which has an absorption cut off of 1,150 nm and band gap of about 1.1 eV, were mainly used in this study to demonstrate the working principle of IR photodetectors although PbS NPs of all other sizes work as well. Direct replacing ZnO NPs by lead sulfide (PbS) NPs in the original device structure however did not yield a working device. It is speculated that the lower LUMO of PbS NPs allows the injection of holes from 4T-TMS into PbS under the strong gate electric field and damaged the channel transport path. Other possibilities that cause the failure of the devices such as incompatible interface of PbS NPs Layer with polystyrene dielectric cannot be excluded. Nevertheless, this issue can be resolved by inserting the ZnO NPs between the PbS NP layer and SiO₂, and the final device structure was shown in Figure 4a. Since the ZnO NPs/PS interface is restored, this device has similar response to UV light with the device shown in Figure 1a. Under IR illumination with a wavelength of 900 nm, the ZnO NPs were not excited directly due to its much larger band gap, while trapped electrons can form at the ZnO/PS interface by the photo-induced electron transfer from PbS to ZnO NPs, as illustrated in Figure 4b. Therefore in addition to regular response to UV light, these devices have response to IR. As shown in Figure 4a, channel current reduction was observed when the photodetector was illuminated by IR light. Although the sensitivity of such IR photodetectors is not optimized yet, the result shown here clearly demonstrated the super-gating mechanism can be used to develop IR sensitive photodetectors by proper device designing. In addition, the result also confirmed that the trapped electrons in the ZnO NPs layer

are responsible for the observed current reduction, and excluded other possible reasons such as UV-irradiation caused organic semiconductor degradation.

Discussion

As for the stability of the detector, permanent damage of the organic materials by the incident UV light, especially deep UV, is possible, which is a widely faced issues in the organic optoelectronic devices, such as organic light-emitting diodes (OLEDs)^{47,48}, organic photovoltaic devices (OPVs)^{49,50}, and photodetectors^{38,51}. In our study, the photodetector do not show visible decay under a UV light illumination of 200 hours with an intensity of 100 nW/cm².

In summary, we have developed a novel NPs super-gated transistor for photon detection and counting with high sensitivity at room temperature. The NPSGOFET device works in a super-float-gating mechanism. The incident photons induce confined electrons beneath the channel layer which tune the current flowing through the transistor channel. The minimum demonstrated detectable UV light intensity was 2.6 photons/μm²s (0.15 nW/cm²) which ranks the NPSGOFET among the best UV photodetectors. The unique memory-like photodetecting process enables the NPSGOFET to count the photons without dead time. A small spacing between the ZnO NPs and the channel region is critical for the high device sensitivity observed. The NPSGOFET devices have huge potential applications for un-cooled, low bias, and low-cost, high-resolution photon detector arrays or photon-manipulated computation.

Methods

Device fabrication. The device structure of the photon counter is schematically shown in Figure 1a. Highly arsenic-doped silicon with a resistivity of 0.001 ~ 0.005 ohm/cm covered with 200 nm thermal grown silicon oxide (SiO₂) was used as gate electrode and dielectric layer, respectively. After UV-ozone treatment of the SiO₂ surface, a ZnO NPs layer with a thickness of about 60 nm was spin coated from a ZnO:chlorobenzene (2.5 wt%) solution at 3000 rpm for 40 s. The ZnO NPs layer was then thermally annealed in air at 260 °C for 30 min.

For the fabrication of the semiconductor film, the trimethyl-[2,5',2'',5''] quater-thiophen-5-yl-silane (4T-TMS) and polystyrene (PS) (9 : 1 by wt) was first dissolved in 1, 2-dichlorobenzene (DCB) (4 mg/ml in all); and then the solution was drop coated on the ZnO surface, during which the substrate was located on a tilted hotplate. The tilting angle was 2.5°, and the drying temperature was 80 °C. During the drying process, there was a vertical phase separation between the PS and 4T-TMS components, which resulted in a bilayer structure of PS/4T-TMS with the PS thin film attached on the ZnO surface. Finally, gold (Au) source and drain electrodes were thermal evaporated with a channel length and width of 100 μm and 1 mm, respectively. The electrical characteristics of the devices were measured using two Keithley 2400 Source Meters in ambient conditions.

Light detecting. The UV light was emitted from deep UV light emitting diodes (LED) with a wavelength of 345 nm (UVTOP®345TO39/TO18FW, Sensor Electronic Technology, Inc.). The photodetector and the UV LED were located in a metal box to exclude the ambient light. The UV intensity was controlled by changing the driving current of the diodes and using neutral filters. The incident light intensity was calibrated with a UV photodetector before applying the filters.

Modeling of device sensitivity versus PS thickness. The influence of the PS thickness (*d*) on the decay rate of the device current under illumination was estimated as below:

- 1) The cross-section of the photon-induced high resistance region (Figure 3a) was:

$$S_c = \pi r_c^2 \quad (6)$$

Here, a critical boundary was defined for the trapping cross-section with a radius of r_c in which within the thermal activation energy of electrons was no more than the potential depth, i.e., $q/4\pi\epsilon_r\epsilon_0\sqrt{d^2+r^2} \geq kT$, where ϵ_r was the relative dielectric constant of PS (2.6), ϵ_0 was the dielectric constant of vacuum, r was the horizontal distance between the hole and the confined electron, k was the Boltzmann constant, and T was the room temperature. A reduced d resulted in an increased r_c and, hence, an increased S_c .

- 2) A reduced PS thickness also resulted in deeper traps which caused larger velocity loss of transporting holes. The maximum value of the depth was:

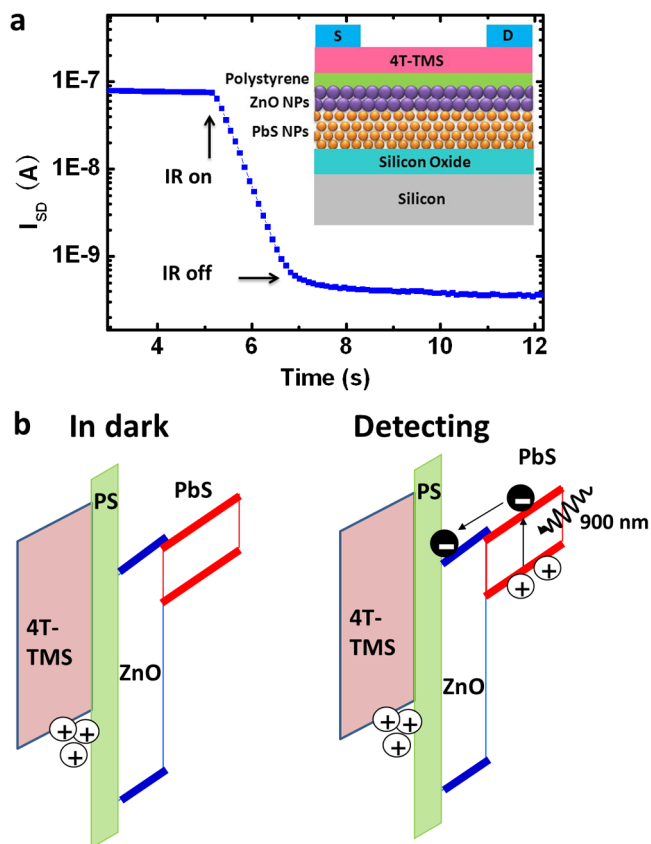


Figure 4 | (a) Exponential channel current decay of the UV-IR NPSGOFET under IR light pulse with a wavelength of 900 nm. Inset is the device structure, where the PbS NPs layer was inserted between the SiO₂ and ZnO NPs layer. (b) Schematic illustration of the detecting process of the UV-IR NPSGOFET photodetector, where the electrons were excited in PbS NPs and then transported into ZnO NPs layer.



$$\Delta E_{\max} = q/4\pi\epsilon_r\epsilon_0 d \quad (7)$$

The decay rates k_{SD} of the NPSGOFET device can be predicted from Eq. (5)–(7) as shown in Figure 3b, where the trap formation efficiency a (38%) was assumed to be equal to the absorbance at 345 nm (Figure 1d).

1. Bennett, C. H. & Brassard, G. Quantum cryptography: Public key distribution and coin tossing, *Proceedings of IEEE International Conference on Computers, Systems and Signal Processing*, Bangalore, India (1984).
2. Gisin, N., Ribordy, G., Tittel, W. & Zbinden, H. Quantum cryptography. *Rev. Mod. Phys.* **74**, 145–195 (2002).
3. Sudharsanan, R. *et al.* Single photon counting Geiger mode InGaAs(P)/InP avalanche photodiode arrays for 3D imaging. *Proceedings of the SPIE, Laser Radar Technology and Applications XIII*. 69500N (2008).
4. Richmond, R. D. & Cain, S. C. *Direct-detection LADAR systems*. (SPIE Press, Washington, 2010).
5. Oh, M. S. *et al.* Development and analysis of a photon-counting three-dimensional imaging laser detection and ranging (LADAR) system. *JOSA A* **28**, 759–765 (2011).
6. Prochazka, I., Hamal, K. & Sopko, B. Recent achievements in single photon detectors and their applications. *J. Mod. Optics* **51**, 1289–1313 (2004).
7. Prochazka, I., Hamal, K. & Kral, L. Single photon counting module for space applications. *J. Mod. Optics* **54**, 151–161 (2007).
8. Mikulec, B. Single photon detection with semiconductor pixel arrays for medical imaging applications. *Doktorarbeit, University of Vienna, Austria* (2000).
9. Webb, S. *The physics of medical imaging*. (CRC Press, Taylor & Francis, 2012).
10. Marino, R. M. *et al.* A compact 3D imaging laser radar system using Geiger-mode APD arrays—System and measurements. *Proceedings of SPIE* **5086**, 1–15 (2003).
11. Hamamatsu Photonics, K. K. Editorial Committee. *Hamamatsu PMT Handbook*. (Hamamatsu Photonics K.K. Press, 2006).
12. Woodard, N. G., Hufstedler, E. G. & Lafyatis, G. P. Photon counting using a large area avalanche photodiode cooled to 100 K. *Appl. Phys. Lett.* **64**, 1177–1179 (1994).
13. Hiskett, P. A. *et al.* Performance and design of InGaAs/InP photodiodes for single-photon counting at 1.55 μm . *Appl. Opt.* **39**, 6818–6829 (2000).
14. Kwiat, P., Steinberg, A., Chiao, R., Eberhard, P. & Petroff, M. High-efficiency single-photon detectors. *Phys. Rev. A* **48**, 867–870 (1993).
15. Sidhu, R. *et al.* GaAsSb resonant-cavity enhanced avalanche photodiode operating at 1.06 μm . *Electron. Lett.* **40**, 1296–1297 (2004).
16. Kim, J., Takeuchi, S., Yamamoto, Y. & Hogue, H. H. Multiphoton detection using visible light photon counter. *Appl. Phys. Lett.* **74**, 902 (1999).
17. Miller, A. J., Nam, S. W., Martinis, J. M. & Sergienko, A. V. Demonstration of a low-noise near-infrared photon counter with multiphoton discrimination. *Appl. Phys. Lett.* **83**, 791 (2003).
18. Fujiwara, M. & Sasaki, M. Multiphoton discrimination at telecom wavelength with charge integration photon detector. *Appl. Phys. Lett.* **86**, 111119 (2005).
19. Rowe, M. A. *et al.* Single-photon detection using a quantum dot optically gated field-effect transistor with high internal quantum efficiency. *Appl. Phys. Lett.* **89**, 253505 (2006).
20. Gansen, E. J. *et al.* Photon-number-discriminating detection using a quantum-dot, optically gated, field-effect transistor. *Nat. Photonics* **1**, 585–588 (2007).
21. Gansen, E. J. *et al.* Operational analysis of a quantum dot optically gated field-effect transistor as a single-photon detector. *IEEE J. Sel. Top. Quant. Electron.* **13**, 967–977 (2007).
22. Rowe, M. *et al.* Analysis of photoconductive gain as it applies to single-photon detection. *J. Appl. Phys.* **107**, 063110 (2010).
23. Guo, F. *et al.* A nanocomposite ultraviolet photodetector based on interfacial trap-controlled charge injection. *Nat. Nanotechnol* **7**, 798–802 (2012).
24. Gong, X. *et al.* High-detectivity polymer photodetectors with spectral response from 300 nm to 1450 nm. *Science* **325**, 1665 (2009).
25. Sukhovatkin, V., Hinds, S., Brzozowski, L. & Sargent, E. H. Colloidal Quantum-Dot Photodetectors Exploiting Multiexciton Generation. *Science* **324**, 1542–1544 (2009).
26. Konstantatos, G. *et al.* Ultrasensitive solution-cast quantum dot photodetectors. *Nature* **442**, 180–183 (2006).
27. Soci, C. *et al.* ZnO nanowire UV photodetectors with high internal gain. *Nano Lett.* **7**, 1003–1009 (2007).
28. Arnold, M. S. *et al.* Broad Spectral Response Using Carbon Nanotube/Organic Semiconductor/C(60) Photodetectors. *Nano Lett.* **9**, 3354–3358 (2009).
29. Jin, Y., Wang, J., Sun, B., Blakesley, J. C. & Greenham, N. C. Solution-processed ultraviolet photodetectors based on colloidal ZnO nanoparticles. *Nano Lett.* **8**, 1649–1653 (2008).
30. Clifford, J. P. *et al.* Fast, sensitive and spectrally tuneable colloidal-quantum-dot photodetectors. *Nat. Nanotechnol* **4**, 40–44 (2008).

31. Koleilat, G. I. *et al.* Efficient, stable infrared photovoltaics based on solution-cast colloidal quantum dots. *ACS Nano* **2**, 833–840 (2008).
32. Lee, J. S., Kovalenko, M. V., Huang, J., Chung, D. S. & Talapin, D. V. Band-like transport, high electron mobility and high photoconductivity in all-inorganic nanocrystal arrays. *Nat. Nanotechnol* **6**, 348–352 (2011).
33. Becerril, H. A., Roberts, M. E., Liu, Z., Locklin, J. & Bao, Z. High-Performance Organic Thin-Film Transistors through Solution-Sheared Deposition of Small-Molecule Organic Semiconductors. *Adv. Mater.* **20**, 2588–2594 (2008).
34. Liu, Z. *et al.* Solution-processed flexible organic transistors showing very-low subthreshold slope with a bilayer polymeric dielectric on plastic. *Appl. Phys. Lett.* **94**, 203301–203303 (2009).
35. Hadfield, R. H. Single-photon detectors for optical quantum information applications. *Nat. Photonics* **3**, 696–705 (2009).
36. Bezryadin, A., Lau, C. & Tinkham, M. Quantum suppression of superconductivity in ultrathin nanowires. *Nature* **404**, 971–974 (2000).
37. Delacour, C. c., Pannetier, B., Villegier, J.-C. & Bouchiat, V. Quantum and Thermal Phase Slips in Superconducting Niobium Nitride (NbN) Ultrathin Crystalline Nanowire: Application to Single Photon Detection. *Nano Lett.* **12**, 3501–3506 (2012).
38. Guo, F., Xiao, Z. & Huang, J. Fullerene Photodetectors with a Linear Dynamic Range of 90 dB Enabled by a Cross-Linkable Buffer Layer. *Adv. Opt. Mater.* (2013).
39. Lao, C. S. *et al.* Giant enhancement in UV response of ZnO nanobelts by polymer surface-functionalization. *J. Am. Chem. Soc.* **129**, 12096–12097 (2007).
40. Bao, Z. & Locklin, J. *Organic Field-Effect Transistors*. (CRC, Boca Raton, 2007).
41. Gartstein, Y. N. & Conwell, E. High-field hopping mobility in molecular systems with spatially correlated energetic disorder. *Chem. Phys. Lett.* **245**, 351–358 (1995).
42. Bässler, H. Charge transport in disordered organic photoconductors a Monte Carlo simulation study. *Phys. Status Solidi B* **175**, 15–56 (2006).
43. Hammock, M. L., Sokolov, A. N., Stoltenberg, R. M., Naab, B. D. & Bao, Z. Organic Transistors with Ordered Nanoparticle Arrays as a Tailorable Platform for Selective, In Situ Detection. *ACS Nano* **6**, 3100–3108 (2012).
44. Khan, H. U. *et al.* In Situ, Label-Free DNA Detection Using Organic Transistor Sensors. *Adv. Mater.* **22**, 4452–4456 (2010).
45. Roberts, M. E., Sokolov, A. N. & Bao, Z. Material and device considerations for organic thin-film transistor sensors. *J. Mater. Chem.* **19**, 3351–3363 (2009).
46. Tsang, S. *et al.* Highly efficient cross-linked PbS nanocrystal/C60 hybrid heterojunction photovoltaic cells. *Appl. Phys. Lett.* **95**, 183505 (2009).
47. Qiu, C., Wang, L., Chen, H., Wong, M. & Kwok, H. Room-temperature ultraviolet emission from an organic light-emitting diode. *Appl. Phys. Lett.* **79**, 2276–2278 (2001).
48. Chao, T. C. *et al.* Highly Efficient UV Organic Light-Emitting Devices Based on Bi (9, 9-diaryluorene) s. *Adv. Mater.* **17**, 992–996 (2005).
49. Li, G. *et al.* High-efficiency solution processable polymer photovoltaic cells by self-organization of polymer blends. *Nat. Mater.* **4**, 864–868 (2005).
50. You, J. *et al.* A polymer tandem solar cell with 10.6% power conversion efficiency. *Nat. Commun.* **4**, 1446 (2013).
51. Ali, F., Periasamy, N., Patankar, M. P. & Narasimhan, K. Integrated Organic Blue LED and Visible-Blind UV Photodetector. *J. Phys. Chem. C* **115**, 2462–2469 (2011).

Acknowledgements

We thank Prof. Zhenan Bao at Stanford University for providing the semiconducting material 4T-TMS for this work. This work is partially supported by the National Science Foundation (Award No. CMM-1265834), Office of Naval Research (ONR, grant No. N000141210556) and Defense Threat Reduction Agency (DTRA) Young Investigator Award (HDTRA1-10-1-0098).

Author contributions

J.H. designed this study; Y.Y. fabricated the devices, carried out the characterizations and simulations. Q.D., B.Y. synthesized the nanoparticles; F.G., cooperated with Q.Z., M.H. in the nano-second UV pulses counting experiment. J.H., Y.Y. wrote the paper.

Additional information

Competing financial interests: The authors declare no competing financial interests.

How to cite this article: Yuan, Y. *et al.* Solution-Processed Nanoparticle Super-Floating-Gated Organic Field-Effect Transistor as Un-cooled Ultraviolet and Infrared Photon Counter. *Sci. Rep.* **3**, 2707; DOI:10.1038/srep02707 (2013).



This work is licensed under a Creative Commons Attribution-NonCommercial-NoDerivs 3.0 Unported license. To view a copy of this license, visit <http://creativecommons.org/licenses/by-nc-nd/3.0>